

# Higgs boson form factor effects in $t\bar{t}$ production by $W^-W^+$ and $ZZ$ fusion.

G.J. Gounaris<sup>a</sup> and F.M. Renard<sup>b</sup>

<sup>a</sup>Department of Theoretical Physics, Aristotle University of Thessaloniki,  
Gr-54124, Thessaloniki, Greece.

<sup>b</sup>Laboratoire Univers et Particules de Montpellier, UMR 5299  
Université Montpellier II, Place Eugène Bataillon CC072  
F-34095 Montpellier Cedex 5, France.

## Abstract

We study the fusion processes  $W^-W^+ \rightarrow t\bar{t}$  and  $ZZ \rightarrow t\bar{t}$  observable at a future  $e^-e^+$  collider and we discuss their sensitivity to an  $Htt$  form factor which may be due to compositeness, in particular when the  $H$  and the top quark have common constituents. We make an amplitude analysis and illustrate which helicity amplitudes and cross sections for specific final  $t\bar{t}$  polarizations are especially sensitive to this form factor.

PACS numbers: 12.15.-y, 12.60.-i, 14.80.-j

# 1 Introduction

The peculiar structure of the standard fermion flavours and of the gauge and Higgs bosons has motivated the search for several types of explanations [1]. Among them one has the possibility of compositeness of particles up to now considered as elementary [2]. The particularly heavy mass of the top quark has suggested that the correspondingly large Higgs-top coupling may be due to Higgs and (possibly partial) top compositeness [3, 4, 5].

If the Higgs boson and the top quark are (even partially) composite, they should both have a form factor. If in addition their constituents are common and do not interact strongly with a vector boson  $V$  (with  $V = \gamma, Z, W$ ), the top quark form factor would not be observed in the usual  $Vtt$  coupling. In such a case only the  $Htt$  form factor could be the right place for the observation of these structures.

But how can we reach the  $Htt$  form factor? Simply through a process where either one top or the H is far off shell, with a variable  $q^2$ . This is a prospect which differs from the search of anomalous  $H$  couplings with on-shell  $H$ .

Which process would be suitable for the observation of such an  $Htt$   $q^2$  dependence? A final  $Ht\bar{t}$  state (like in  $e^-e^+ \rightarrow Ht\bar{t}$ ) would not be a priori adequate, the final  $H$  being on shell. One should for example look for a process with an intermediate H with a variable  $q^2$  and a final  $t\bar{t}$  pair.

At a muon collider, the process  $\mu^-\mu^+ \rightarrow H \rightarrow t\bar{t}$  would be the simplest one for this purpose, but it is too weak as compared to  $\mu^-\mu^+ \rightarrow V \rightarrow t\bar{t}$ , which completely dominates the  $t\bar{t}$  production data. At LHC  $gg \rightarrow H \rightarrow t\bar{t}$  is also too weak as compared to other (pure QCD)  $gg \rightarrow t\bar{t}$  contributions.

We have therefore considered the fusion processes  $W^-W^+, ZZ \rightarrow t\bar{t}$  which contain the  $W^-W^+, ZZ \rightarrow H \rightarrow t\bar{t}$  contributions. In the Standard Model (SM), these fusion processes have been studied for a long time [6, 7, 8]. But now we want to see the influence of a modification of the Higgs boson exchange term, in particular through a form factor. We have therefore recomputed the  $W^-W^+, ZZ \rightarrow t\bar{t}$  amplitudes including, in addition to the  $(W^-W^+, ZZ) \rightarrow H \rightarrow t\bar{t}$  contribution, the corresponding  $b, t$  exchanges in  $t$  or  $u$  channels, and the photon and  $Z$  exchanges in the  $s$  channel. In SM they are all of comparable size.

We have studied the sensitivity of these fusion processes to the  $H$  contribution, especially when there is a  $q^2$ -dependent departure from the pointlike SM  $Htt$  coupling. In fact this applies also to a more general situation in which the products  $g_{HWW}g_{Htt}$  and  $g_{HZZ}g_{Htt}$  get a  $q^2$ -dependence.

Using these, a peculiar sensitivity appears when the initial vector bosons  $W^-W^+$  or  $ZZ$  are both longitudinal (LL), because of the famous gauge cancellations at high energies, which are now perturbed by Higgs boson form factors. In order to appreciate the importance of this effect, we illustrate the behavior of the various amplitudes and cross sections for transverse or longitudinal gauge bosons and for polarized or unpolarized final  $t\bar{t}$  states. We insist on the importance of separating the various final state polarizations, in order to identify the origin of a possible departure from the SM prediction.

In these illustrations we compare the SM case with pointlike H couplings, to some

examples of  $q^2$ -dependence. In order to be quantitatively significant of a form factor effect (and not simply of a change of normalization due to an anomalous coupling) these examples are constrained to coincide at  $q^2 = m_H^2$  with the SM value. Moreover, they should also satisfy the high energy cancellation of LL amplitudes. We use effective forms satisfying these two requirements.

Such fusion processes can be observed at a future [9]  $e^-e^+$  collider in  $e^-e^+ \rightarrow \nu\bar{\nu}t\bar{t}$  and  $e^-e^+ \rightarrow e^+e^-t\bar{t}$ . The corresponding cross sections can be easily obtained by integrating the subprocesses with the luminosity factors given by the leading effective weak boson approximation (LEWA). In the illustrations we use the luminosity factors of [7] and [10] (where the possibility of polarized  $e^-e^+$  beams has also been considered, which though does not seem to help for increasing the sensitivity to the  $Htt$  form factor).

In the  $e^-e^+ \rightarrow e^-e^+t\bar{t}$  case we add to the  $ZZ \rightarrow t\bar{t}$  subprocess, the background contributions of the  $\gamma\gamma \rightarrow t\bar{t}$ ,  $\gamma Z \rightarrow t\bar{t}$ ,  $Z\gamma \rightarrow t\bar{t}$  subprocesses, which do not contain  $H$  effects.

These fusion processes also occur at LHC but with large backgrounds such that special studies should be done with careful detection characteristics.

In Sec. II we treat the  $W^-W^+ \rightarrow t\bar{t}$  and  $ZZ \rightarrow t\bar{t}$  processes in SM. In Sec. III we describe possible expressions for the  $Htt$  form factor. In Sec. IV we discuss and illustrate the behavior of the various amplitudes and cross sections and their sensitivity to the  $Htt$  form factor. In Sec. V we summarize our comments and list possible improvements and developments. An Appendix collects the explicit expressions of the various helicity amplitudes.

## 2 SM analysis of $W^-W^+ \rightarrow t\bar{t}$ and $ZZ \rightarrow t\bar{t}$ .

We express the amplitudes

$$W^-(\epsilon, \lambda, l) + W^+(\epsilon', \lambda', l') \rightarrow t(\tau, p) + \bar{t}(\tau', p') \quad , \quad (1)$$

in terms of the  $W^\mp$  polarization vectors, helicities and momenta respectively denoted as  $(\epsilon, \lambda, l)$  and  $(\epsilon', \lambda', l')$ ; as well as the  $t, \bar{t}$  helicities and momenta denoted as  $(\tau, p)$  and  $(\tau', p')$  (see the Appendix). By  $\theta$  we denote the center of mass angle between the  $W^-(\epsilon, \lambda, l)$  and  $t(\tau, p)$  directions of motion, and we also define

$$\begin{aligned} s &= q^2 = (l + l')^2 = (p + p')^2 \quad , \\ t &= q_t^2 = (l - p)^2 = (l' - p')^2 \quad , \quad u = q_u^2 = (l' - p)^2 = (l - p')^2 \quad . \end{aligned} \quad (2)$$

The Born level amplitude is written as

$$A = A_u^{WW} + A_{s,\gamma}^{WW} + A_{s,Z}^{WW} + A_{s,H}^{WW} \quad , \quad (3)$$

in terms of the four diagrammatic contributions induced by

the u-channel bottom exchange

$$A_u^{WW} = \frac{-e^2 g_{Wtb}^L}{q_u^2 - m_b^2} \bar{u}(t) [\not{\epsilon}' P_L (\not{q}_u + m_b) \not{\epsilon} P_L] v(\bar{t}) \quad , \quad (4)$$

with  $g_{Wtb}^L = 1/(s_W \sqrt{2})$  ,

the s-channel  $V = \gamma, Z$  exchange

$$A_{s,V}^{WW} = \frac{-e^2 g_V}{s - m_V^2 + im_V \Gamma_V} \bar{u}(t) [2(\epsilon.l') \not{\epsilon}' + 2(\epsilon.l) \not{\epsilon} - (\epsilon.\epsilon') (\not{l}' - \not{l})] (g_{Vt}^L P_L + g_{Vt}^R P_R) v(\bar{t}) \quad , \quad (5)$$

with

$$g_\gamma = 1 \quad , \quad g_Z = \frac{c_W}{s_W} \quad , \quad g_{\gamma t}^L = g_{\gamma t}^R = \frac{2}{3} \quad , \quad g_{Zt}^L = \frac{1}{2s_W c_W} \left( 1 - \frac{4s_W^3}{3} \right) \quad , \quad g_{Zt}^R = -\frac{2s_W}{3c_W} \quad , \quad (6)$$

and s-channel H exchange

$$A_{s,H}^{WW} = \frac{-e^2 g_{HWW} g_{Htt}}{s - m_H^2 + im_H \Gamma_H} (\epsilon.\epsilon') [\bar{u}(t) v(\bar{t})] \quad , \quad (7)$$

with

$$g_{Htt} = -\frac{m_t}{2s_W m_W} \quad , \quad g_{HWW} = \frac{m_W}{s_W} \quad .$$

The 36 helicity amplitudes  $F_{\lambda,\lambda',\tau,\tau'}(s,\theta)$  implied by (3), are listed in the Appendix using the standard forms of Dirac spinors and vector boson helicities<sup>1</sup> [11]. These contain the 10 helicity conserving (HC) amplitudes which satisfy the rule [12]  $\lambda + \lambda' = \tau + \tau'$ , and the 26 helicity violating (HV) ones which violate it. Only 6 of them contain an  $H$  exchange contribution. Note that CP conservation imposes the relation

$$F_{\lambda,\lambda',\tau,\tau'}(s,\theta) = F_{-\lambda',-\lambda,-\tau',-\tau}(s,\theta) \quad . \quad (8)$$

In terms of the aforementioned helicity amplitudes, the cross sections for specific  $W^-$ ,  $W^+$  and  $t, \bar{t}$  helicities are written as

$$\frac{d\sigma(W_\lambda^- W_{\lambda'}^+ \rightarrow t_\tau \bar{t}_{\tau'})}{d\cos\theta} = \frac{3p_t}{32\pi l_W s} |F_{\lambda,\lambda',\tau,\tau'}(s,\theta)|^2 \quad , \quad (9)$$

involving (2) and the magnitudes of the  $t$  and  $W$  c.m. momenta

$$p_t = \sqrt{\frac{s}{4} - m_t^2} \quad , \quad l_W = \sqrt{\frac{s}{4} - m_W^2} \quad . \quad (10)$$

---

<sup>1</sup>The transverse (T)  $\lambda, \lambda' = -1, +1$  and longitudinal (L)  $\lambda, \lambda' = 0$  helicities are obtained from the corresponding  $W^\mp$  polarization vectors  $\epsilon, \epsilon'$ .

We next turn to the corresponding cross sections for  $e^-e^+ \rightarrow \nu\bar{\nu}t\bar{t}$  obtained by multiplying each  $(\lambda, \lambda')$  contribution to (9) by the corresponding luminosity factor

$$L_{\lambda, \lambda'}(y) = \int_y^1 \frac{dx}{x} f_{W^-, \lambda}(x) f_{W^+, \lambda'}\left(\frac{y}{x}\right) , \quad (11)$$

computed with the  $W^\mp$  distribution functions as given in [7, 10], with  $y = s/(4E^2)$  and  $E$  being the c.m.  $e^\mp$  beam energy. The integration limits  $(y, 1)$  can be modified to  $(x_{min}, x_{max})$  when kinematical detection cuts are applied. As in the parton model, in the leading approximation the  $W^\mp$  vector bosons are emitted along the  $(e^-, e^+)$  axis, so that the final  $(t, \bar{t})$  direction in their center of mass is also given by the same angle  $\theta$ , as the one defined just before (2).

The  $e^-e^+$  cross sections

$$\frac{d\sigma_{e^-e^+}(\tau, \tau')}{dy d\cos\theta} = \sum_{\lambda, \lambda'} L_{\lambda, \lambda'}(y) \frac{d\sigma(W_\lambda^- W_{\lambda'}^+ \rightarrow t_\tau \bar{t}_{\tau'})}{d\cos\theta} , \quad (12)$$

are also computed for specific final  $t, \bar{t}$  polarizations or, by summing them, for an unpolarized final state.

For the  $ZZ \rightarrow t\bar{t}$  process, the notation is the same as for  $W^-W^+$ . Explicitly, we now have

$$Z(\epsilon, \lambda, l) + Z(\epsilon', \lambda', l') \rightarrow t(\tau, p) + \bar{t}(\tau', p') , \quad (13)$$

but different diagrams now occur involving no s-channel  $(\gamma, Z)$  exchange, but both  $u$ - and  $t$ -channel top exchange contributions given by

$$\begin{aligned} A_u^{ZZ} &= \frac{-e^2}{q_u^2 - m_t^2} \bar{u}(t) [\not{\epsilon}'(g_{Zt}^L P_L + g_{Zt}^R P_R)(\not{q}_u + m_t) \not{\epsilon}(g_{Zt}^L P_L + g_{Zt}^R P_R)] v(\bar{t}) , \\ A_t^{ZZ} &= \frac{-e^2}{q_t^2 - m_t^2} \bar{u}(t) [\not{\epsilon}(g_{Zt}^L P_L + g_{Zt}^R P_R)(\not{q}_t + m_t) \not{\epsilon}'(g_{Zt}^L P_L + g_{Zt}^R P_R)] v(\bar{t}) , \end{aligned} \quad (14)$$

as well as s-channel  $H$  exchange contributions

$$A_{s,H}^{ZZ} = \frac{-e^2 g_{HZZ} g_{Htt}}{s - m_H^2 + im_H \Gamma_H} (\epsilon.\epsilon') [\bar{u}(t)v(\bar{t})] , \quad (15)$$

involving  $g_{Htt} = -m_t/(2s_W m_W)$  ,  $g_{HZZ} = m_Z/(s_W c_W)$ .

The above  $u$ - and  $t$ -channel top exchange expressions are also used for describing the  $\gamma\gamma \rightarrow t\bar{t}$ ,  $\gamma Z \rightarrow t\bar{t}$ ,  $Z\gamma \rightarrow t\bar{t}$  processes, by adapting the  $g_{Zt}^{L,R}$  couplings in (6). These processes do not involve the  $H$  exchange diagram and the  $Htt$  form factor. They constitute a background to be added to  $ZZ \rightarrow t\bar{t}$ , when we consider the  $e^+e^- \rightarrow e^+e^-t\bar{t}$  process.

The corresponding  $e^-e^+ \rightarrow e^-e^+t\bar{t}$  cross section is obtained as in the previous  $W^-W^+$  case and (11) and (12), by using the  $Z$  and  $\gamma$  distribution functions also given in [7, 10]. In the present work we give results with and without the  $\gamma\gamma \rightarrow t\bar{t}$ ,  $\gamma Z \rightarrow t\bar{t}$ ,  $Z\gamma \rightarrow t\bar{t}$  backgrounds.

### 3 Higgs boson form factor effects

The simplest Higgs boson form factor effect comes through the products of couplings  $g_{HWW}g_{Htt}$ ,  $g_{HZZ}g_{Htt}$  in (7) and (15), when they get an anomalous  $q^2$  dependence. This may simply be due to the presence of an  $Htt$  form factor in  $g_{Htt}$ , or to the simultaneous presence of  $Htt$  and of  $HWW$ ,  $HZZ$  form factors.

Let us first insist on the difference between such a form factor effect and the presence of anomalous couplings. Anomalous couplings are usually described by effective high dimension operators generated by new interactions with a new physics scale  $\Lambda$  higher than the available energy. In the case of  $Htt$  see for example [13]. The effect of each of such operators is a departure from the SM couplings already appearing on shell and behaving like powers of  $q^2/\Lambda^2$ .

Our form factor description of compositeness effects assumes that the on-shell SM value is reproduced by the compositeness structure, but that a complete  $q^2$  dependence is generated even within the new physics domain. It could possibly be described by an involved sum of effective operators with different dimensions.

As we only study the observability of effects of the presence of a form factor, and not of a single anomalous coupling modifying the SM on-shell value of the coupling, we use an effective form factor generating some  $q^2$  dependence, but imposing the SM value at  $q^2 = m_H^2$ .

In the spirit of compositeness, a typical  $q^2$  dependence of the  $Htt$  vertex may be given by an  $STS$  or a  $TST$  triangular loop (where  $S$  and  $T$  are new scalar or fermion constituents of mass  $m$ ).

The crude result, imposing the SM normalization value at  $q^2 = m_H^2$  to the product of couplings, would be

$$g_{Htt}^0(q^2) = g_{Htt}^{SM} \frac{C(q^2)}{C(m_H^2)} \quad , \quad (16)$$

where in the  $STS$  case we have

$$C(q^2) = m_t(C_0(q^2) + C_{12}(q^2) - C_{11}(q^2)) + mC_0(q^2) \quad , \quad (17)$$

in terms of Passarino-Veltman functions [14], while in the  $TST$  case we have

$$\begin{aligned} C(q^2) &= \kappa(q^2) + q^2 C_{12}(q^2) + m^2 C_0(q^2) + 2m_t m (C_{12}(q^2) - C_{11}(q^2)) \quad , \\ \kappa(q^2) &= m_t^2 (C_{21}(q^2) + C_{22}(q^2)) - 2C_{23}(q^2) + q^2 C_{23}(q^2) + 4C_{24}^r(q^2) \quad , \end{aligned} \quad (18)$$

where  $C_{24}^r(q^2)$  is a divergence free quantity (for example as given by the SRS scheme [15]).

However such choices would destroy the cancellation of LL amplitudes at high  $(s, t, u)$ -values, so that they cannot correspond to a viable model. There are various ways to recover the cancellation. They may for example depend on the assumption of partial or total fermion compositeness, in addition to Higgs compositeness. This will correspondingly affect the  $b$ ,  $t$  and  $V$  exchanges and/or  $H$  exchange amplitudes. In any case these additional contributions should combine with the contribution involving the Higgs form factor in such a way that the total satisfies unitarity, i.e. does not explode at high energy.

There may be various such acceptable results which would quantitatively differ from the standard case. The minimal change would correspond to an effective value which becomes similar to the SM one at high  $q^2$ . As our aim is only to study the sensitivity of the considered processes to the occurrence of form factors, we choose an arbitrary effective  $q^2$  expression which satisfies the above minimal requirement. Any other choice should give larger differences with the SM prediction.

One example is

$$g_{Htt}^{eff}(q^2) = g_{Htt}^{SM} \left\{ \frac{C(q^2)}{C(m_H^2)} + \frac{q^2 - m_H^2}{q^2 + 4m^2} \left(1 - \frac{C(q^2)}{C(m_H^2)}\right) \right\} , \quad (19)$$

where either (17) or (18) are used, respectively producing the STS and TST *effective* model variations.

Another (trivial) possibility could be the occurrence of one (or more) resonance ( $H'$ ), located at intermediate  $q^2$  values. The corresponding contribution

$$A_{s,H'}^{WW,ZZ} = \frac{-e^2 g_{H'XX} g_{H'tt}}{q^2 - m_{H'}^2 + im_{H'}\Gamma_{H'}} (\epsilon.\epsilon') [\bar{u}(t)v(\bar{t})] , \quad (20)$$

with  $X = W$  or  $Z$ , corresponds to a form factor effect written as

$$g_{Htt}^{eff}(q^2) = g_{Htt} + g_{H'tt} \frac{g_{H'XX}(q^2 - m_H^2 + im_H\Gamma_H)}{g_{HXX}(q^2 - m_{H'}^2 + im_{H'}\Gamma_{H'})} , \quad (21)$$

and satisfying the constraint

$$g_{Htt} g_{HXX} + g_{H'tt} g_{H'XX} = g_{Htt}^{SM} g_{HXX}^{SM} , \quad (22)$$

so that the high energy cancellation is obeyed.

The shapes of the Re and Im parts of such form factors are shown in Figs. 1(a) and (b) where we have arbitrarily chosen three examples: the *crude STS* case based on (16) and (17), the *effective* case based on (17) and (19), both with a constituent mass  $m = 0.5$  TeV, and the *resonance* case based on (20) and the mass-choice<sup>2</sup>  $m_{H'} = 0.75$  TeV. In these figures, one can see in particular the differences of the high energy behavior in both real [Fig.1(a)] and imaginary [Fig.1(b)] parts of the form factor. The corresponding effects in amplitudes and cross sections are illustrated below.

## 4 Properties of amplitudes and cross sections.

The basic results for total SM cross sections have been given in [7]. Here we present a detailed amplitude analysis, in order to provide an understanding of the modifications resulting from the presence of new  $q^2$  dependencies in the  $H$  exchange term.

---

<sup>2</sup>This choice was initiated by a signal seen in the 2015 data [16, 17], which meanwhile has disappeared [18]. In any case though it may still be used as an example.

## 4.1 The $W_\lambda^- W_{\lambda'}^+ \rightarrow t_\tau \bar{t}_{\tau'}$ process.

We discuss separately the pure transverse (TT), the mixed (TL, LT) and the pure longitudinal (LL) amplitudes. Since in SM there are specific strong cancellations between the various terms contributing to the (TL, LT) and to the (LL) amplitudes, they correctly behave at high energy.

During this analysis we also check the helicity conservation rule valid in SM at tree level [12], but not in the presence of arbitrary form factors.

The ten HC amplitudes are

$$F_{-++}, F_{-+-}, F_{+--}, F_{+-+}, F_{0---} = F_{+0++}, F_{-0--} = F_{0+++}, F_{00-+}, F_{00+-} \quad , \quad (23)$$

while the 26 HV ones, which are suppressed at high energy in the pure SM case, are

$$\begin{aligned} F_{----} &= F_{++++}, F_{---+} = F_{++--}, F_{-+-+} = F_{-++-} = F_{+---} = F_{+--+}, \\ F_{0-++} &= F_{+0--}, F_{0--+} = F_{+0-+}, F_{0-+-} = F_{+0+-}, F_{-0++} = F_{0+--}, \\ F_{-0-+} &= F_{0+--}, F_{-0+-} = F_{0+--}, \end{aligned} \quad (24)$$

$$F_{-----} = F_{++++}, F_{----+} = F_{++--}, F_{00++} = F_{00--} \quad . \quad (25)$$

Figure 2 presents the HC amplitudes (23) in the upper panels, while the HV amplitudes of (24) are shown in the lower panels. The left panels refer to TT  $W^-W^+$ , while right panels always involve at least one longitudinal  $W^\mp$ . Both of these sets do not involve any s-channel H exchange, so there is no effect of the form factor. At high energy the HC amplitudes have weak energy dependencies and no or negligible imaginary parts. The leading ones are  $F_{-++}, F_{+--}, F_{0---} = F_{+0++}$  and  $F_{00-+}, F_{00+-}$ , with a high energy limiting absolute value of the order of 0.05 to 0.6. Concerning particularly  $F_{00-+}, F_{00+-}$ , we note that they acquire their high energy magnitude after a strong cancellation between the u-channel bottom exchange and s-channel  $\gamma, Z$  exchange contributions. We also note that the HV amplitudes in the lower panels of Fig.2, involve high energy cancellations among a u-channel bottom exchange and an s-channel  $\gamma, Z$  exchange, and decrease with the energy. These HV amplitudes are smaller than the HC ones shown in the upper panels.

We next turn to the six HV amplitudes appearing in (25), which are the only ones receiving an  $H$  exchange contribution, and being therefore sensitive to the  $Htt$  form factor. These are shown in Fig.3, where the standard amplitudes involving the SM pointlike  $Htt$  coupling, are compared to those induced by the examples of anomalous  $Htt$  form factors shown in Fig.1. These  $H$  sensitive amplitudes are of variable size. The four (TT) ones listed in the upper and middle panels of Fig.3, are almost 10 times smaller than the leading "no H" ones shown in Fig.2.

The two (LL) ones, appearing in the lower panels of Fig.3, can reach much larger values. One can see the specific energy dependencies in the *effective* and *resonance* cases. Imaginary parts may be important above the "new" threshold or around the resonance. The sensitivity of the four (TT) amplitudes to the  $Htt$  form factor is not as strong as the sensitivity of the two (LL) ones. The chosen form factor leads to modifications of these amplitudes for  $s \gtrsim (m^2, m_H^2)$  (the new scale) and mostly at higher energies, although they satisfy the cancellation at very high energies.



In addition to the modification of the amplitudes around  $(m^2, m_{H'}^2)$  by the form factor effect, a strong absence of cancellation effect would appear at high energy in the *crude STS* form factor choice. With the other choice (the "effective" one satisfying the cancellation constraint) there still remains a strong departure from the SM prediction. So these LL amplitudes,  $F_{00++} = F_{00--}$ , are the clearest source of large sensitivity to the  $Ht\bar{t}$  form factor.

**Form factor sensitivity of the  $d\sigma(e^-e^+ \rightarrow \nu\bar{\nu}t_\tau\bar{t}_{\tau'})/d\cos\theta$  cross sections:** These cross sections would reflect the above amplitude properties. In this case, for each final  $t_\tau\bar{t}_{\tau'}$  polarization, we have to sum the different  $W_\lambda^-W_{\lambda'}^+$  initial state contributions, each probability being multiplied by the corresponding luminosity (11). This sum involves all HV and HC amplitudes, even those which do not contain the  $H$  contribution, thereby diminishing the relative size of the form factor effect. In Fig.4 we thus present the following illustrations:

- In the upper panel we show the energy dependencies of the left-right ( $\tau = -\tau' = -1/2$ ) and right-left ( $\tau = -\tau' = 1/2$ ) differential cross sections at  $\theta = 60^\circ$ . There exists no H contribution to these quantities.
- In the middle panels we show the left-left ( $\tau = \tau' = -1/2$ ) and right-right ( $\tau = \tau' = 1/2$ ) differential cross sections, again at  $\theta = 60^\circ$ .
- Finally, in the lower panels we give the energy (at  $\theta = 60^\circ$ ) and the angular (at  $\sqrt{s} = 1\text{TeV}$ ) dependencies, when the  $t\bar{t}$ -helicities are not observed.

The results in the middle and lower panels of Fig.4 do depend in the  $Ht\bar{t}$  form factor. In them, one recognizes the strong threshold or resonance effects seen in the amplitudes in Fig.3 around  $s \simeq (m^2, m_{H'}^2)$  and higher energies.

As expected, the form factor effects in the lower panels of Fig.4 are somewhat smaller than those in the middle panels, since the first also involve amplitudes insensitive to  $H$ .

In the right lower panel of Fig.4 we also show the angular dependence in the unpolarized case at  $\sqrt{s} = 1\text{TeV}$ . One can see that the  $H$  contribution gives an additional typical constant angular dependence, which differs from the backward peaking of the dominating  $u$  channel exchange. The effect is therefore mainly localized in the forward and central domain.

Finally we have also computed the integrated cross sections for some examples of the  $e^\mp$  c.m. energy  $E_e$ , with the  $t\bar{t}$  invariant mass chosen larger than some minimal value  $\sqrt{s} > \sqrt{s_{min}}$ . In this case we have imposed an angular cut in order to eliminate the main background coming from photon radiation, in agreement with the study of [19]. Thus

- for  $E_e = 1\text{TeV}$  and  $\sqrt{s_{min}} = 2m_t$  or  $1\text{TeV}$ , one gets integrated cross sections of 0.10 or 0.03 fb in SM, and 6.1 or 0.17 fb in the presence of the form factor;
- while for  $E_e = 3\text{TeV}$  and  $\sqrt{s_{min}} = 2m_t$  or  $1\text{TeV}$ , one gets integrated cross sections of 3.8 or 1.2 fb in SM, and 72. or 5.8 fb in the presence of the form factor.

These dependencies can easily be understood from the shapes of the corresponding energy dependencies of the SM and the form factor effects shown in Fig.4. Accordingly, for the energies of a future collider, (see for example Fig.1 of [20] and its Refs.[1-4] a luminosity of  $10^{35}\text{cm}^{-2}\text{s}^{-1}$  would give  $10^2$  to  $10^5$  events per year (depending on the energies and the cuts) and a large observability of form factor effects.

## 4.2 The $Z_\lambda Z_{\lambda'} \rightarrow t_\tau \bar{t}_{\tau'}$ process.

The properties of the various helicity amplitudes for  $Z_\lambda Z_{\lambda'} \rightarrow t_\tau \bar{t}_{\tau'}$  are globally similar to those of the  $W^-W^+$  case. The cancellations for longitudinal amplitudes are also similar to those for  $W^-W^+$ , but it now occurs between the  $t$  and  $u$  channel top exchange (there is no  $\gamma, Z$  exchange), and also with the  $s$ -channel H exchange in the  $F_{00++} = F_{00--}$  case. These later amplitudes are the leading ones, with the larger sensitivity to the form factor.

Following a similar a procedure as for the previous case<sup>3</sup>, we present in Fig.5 the insensitive to the H form factor amplitudes, with upper panels describing the tree level SM HC amplitudes,

$$F_{-+-+}, F_{-++-}, F_{+--+}, F_{+---}, F_{0---} = F_{+0++}, F_{-0--} = F_{00++}, F_{00-+} \quad , \quad (26)$$

and the lower panels showing the HV ones

$$\begin{aligned} F_{-----} &= F_{++++}, F_{----+} = F_{++++-}, F_{-+---} = F_{-++++} = F_{+----} = F_{+----+}, \\ F_{0-++} &= F_{+0--}, F_{0--+} = F_{+0-+}, F_{0-+-} = F_{+0+-}, F_{-0++} = F_{0+--}, \\ F_{-0-+} &= F_{0+--}, F_{-0+-} = F_{0+--} \quad . \end{aligned} \quad (27)$$

The amplitudes in Fig.5 are all real.

Correspondingly, Fig.6 shows the three H-form factor sensitive amplitudes in

$$F_{-----} = F_{++++}, F_{----+} = F_{++++-}, F_{00++} = F_{00--} \quad , \quad (28)$$

in the upper, middle and lower panels respectively. The same form factor models as in Fig.1 are used. Left and right panels are respectively giving the real and imaginary parts of these amplitudes.

A source of differences between the  $ZZ$  and the  $W^-W^+$  case is the weaker  $Ztt$  couplings which lead to a weaker SM (non-H) contribution and therefore a relatively larger sensitivity to the  $Htt$  form factor, both around  $s \simeq (m^2, m_{H'}^2)$  and higher energy.

But the largest differences come from the  $ZZ$  symmetry, which renders the angular distribution symmetric with respect to  $\theta \rightarrow \pi - \theta$ . This leads in particular to the presence of both forward and backward peaking of the non-H contribution. Both features lead to a large sensitivity to  $H$  exchange in the central domain.

A priori the comparison of the  $W^-W^+$  and  $ZZ$  processes would contribute to the identification of a possible nonstandard  $Htt$  effect.

---

<sup>3</sup>Compare Fig.2

**Form factor sensitivity of the  $d\sigma(e^-e^+ \rightarrow e^-e^+t_\tau\bar{t}_{\tau'})/d\cos\theta$  cross sections:** The new point is now that the  $ZZ$  process gets large background effects from  $\gamma\gamma \rightarrow t\bar{t}$ ,  $\gamma Z \rightarrow t\bar{t}$  and  $Z\gamma \rightarrow t\bar{t}$  processes which have no  $H$  contribution. This background is essentially dominated by the  $\gamma\gamma \rightarrow t\bar{t}$  contribution. It can however be reduced by detecting the final  $e^-e^+$  and making an angular cut rejecting their big forward contribution.

In the following illustrations we have taken a background example obtained with a tentative cut at  $\theta = 0.1$ . This reduces the background which is then only one order of magnitude larger than the SM pure  $ZZ$  contribution. We thus successively show the effects in the polarized (Figs.7 and 8) and in the unpolarized (Fig.9)  $t\bar{t}$  cross sections.

Figure 7 presents H-independent cross sections for  $\tau = -\tau'$  showing the relative importance of the background contribution.

Figure 8 presents then the H-dependent cross sections for  $\tau = \tau'$  showing that the modifications of the  $ZZ$  contributions due to H form factors can nevertheless be observable (locally in the case of a resonance or in the high energy behavior in the case of an effective form) even with the presence of the background.

Finally in Fig.9 we present the unpolarized cross sections. The upper panels give energy dependencies and the lower panels the angular ones. It appears that even in this unpolarized case, effects of effective or resonance contributions can then be clearly seen, at the (20%-50%) level with the chosen parameters, mostly in the central angular region.

As in the previous subsection, we have also computed the integrated cross sections for  $ZZ + \text{background}$  with the same examples of electron  $e^\mp$  energy  $E_e$ , minimal  $t\bar{t}$  invariant mass  $\sqrt{s_{min}}$  and cuts. Thus

- for  $E_e = 1$  TeV and  $\sqrt{s_{min}} = 2m_t$  or 1 TeV, one gets total ( $ZZ + \text{background}$ ) integrated cross sections values of 0.92 or 0.023 fb in SM, and 0.92 or 0.031 fb with the form factor;
- while for  $E_e = 3$  TeV and  $\sqrt{s_{min}} = 2m_t$  or 1 TeV, one gets integrated cross sections values of 7.2 or 0.5 fb in SM, and 7.2 or 0.8 fb with the form factor.

These dependencies can also be understood from the shapes of the corresponding energy dependencies in Fig.9, in particular the large sensitivity to the minimal  $t\bar{t}$  invariant mass. Although the sensitivity to the form factor effects is weaker than in the  $WW$  case, these  $ZZ + \text{background}$  results, with  $10^2$  to  $10^4$  events in a future collider [20], could still correspond to observable situations.

Of course these illustrations just correspond to arbitrary examples. Detection characteristics should be adapted to the real observations.

## 5 Final comments and possible developments.

We have shown what could be the effect of a  $Htt$  form factor on the energy and angular dependencies of the amplitudes and cross sections of the  $W^-W^+ \rightarrow t\bar{t}$  and  $ZZ \rightarrow t\bar{t}$

fusion processes, especially when identifying the final  $t\bar{t}$  polarizations.

For the illustrations we have taken simple expressions of form factors, for example arising from common constituents of the Higgs boson and the top quark. We have chosen effective expressions satisfying normalization constraints and leading to acceptable high energy behavior of the amplitudes. For comparison we have also shown the spectacular effect generated by a new resonance form.

By using the relevant LEWA functions of [6, 7, 10] we have seen how the above sensitivity of the  $W^-W^+ \rightarrow t\bar{t}$  and  $ZZ \rightarrow t\bar{t}$  subprocesses is transmitted to the  $e^-e^+ \rightarrow \nu\bar{\nu}t\bar{t}$  and  $e^-e^+ \rightarrow e^-e^+t\bar{t}$  cross sections. For the  $ZZ$  case we have added the background contributions of the  $\gamma\gamma \rightarrow t\bar{t}$ ,  $\gamma Z \rightarrow t\bar{t}$ ,  $Z\gamma \rightarrow t\bar{t}$  subprocesses which do not contain  $H$  effects. This background can be reduced by applying angular cuts to the detection of the final  $e^-e^+$ .

A large sensitivity to the  $Htt$  form factor is observed in the energy and angular dependencies of these cross sections. With the expected values of the future colliders energy and luminosity, a large number of events is expected leading to a good observability of the form factor effects. Measurements of the final  $t\bar{t}$  polarizations would increase this sensitivity and help for the identification of the origin of a possible departure from the SM predictions.

Applications to LHC may also be considered with  $W^-W^+ \rightarrow t\bar{t}$  and  $ZZ \rightarrow t\bar{t}$  fusion, after emission of  $W$  and  $Z$  by  $q$  and  $\bar{q}$  partons; but there are many other subprocesses creating  $t\bar{t}$  pairs which will overwhelm these fusion ones. Involved sets of detection features may help to separate them, but this is beyond our competence.

## Appendix: The helicity amplitudes $F_{\lambda,\lambda',\tau,\tau'}(s, \theta)$

The usual Dirac spinor decomposition is made for  $\tau, \tau'$  helicities of the top and antitop with momenta  $p^\mu = (p_t^0, p_t \sin \theta, 0, p_t \cos \theta)$  and  $p'^\mu = (p_t^0, -p_t \sin \theta, 0, -p_t \cos \theta)$ :

$$\bar{u}(p, \tau) = \sqrt{E_t + m_t}(\chi_\tau^+, -2\tau r_t \chi_\tau^+), \quad v^T(p', \tau') = -\sqrt{E_t + m_t}(r_t \chi_{\tau'}^-, -2\tau' \chi_{\tau'}^-), \quad (\text{A.1})$$

with

$$r_t = \frac{p_t}{E_t + m_t}, \quad \chi_+^+ = \left( \cos \frac{\theta}{2}, \sin \frac{\theta}{2} \right), \quad \chi_-^+ = \left( -\cos \frac{\theta}{2}, \sin \frac{\theta}{2} \right). \quad (\text{A.2})$$

For the No.1 gauge boson according to the standard Jacob-Wick (JE) convention [11]  $V = W^-, Z$ , with momentum  $l^\mu = (l^0, 0, 0, l)$ , the transverse and longitudinal polarization vectors are respectively given by

$$\epsilon^\mu(l, \lambda) = \left( 0, \frac{-\lambda}{\sqrt{2}}, \frac{-i}{\sqrt{2}}, 0 \right), \quad \epsilon^\mu(l, 0) = \left( \frac{l}{m_V}, 0, 0, \frac{l^0}{m_V} \right), \quad (\text{A.3})$$

while for the No.2  $V' = W^+, Z$ , with momentum  $l'^\mu = (l^0, 0, 0, -l)$ , the corresponding polarization vectors are

$$\epsilon'^\mu(l', \lambda') = \left(0, \frac{\lambda'}{\sqrt{2}}, \frac{-i}{\sqrt{2}}, 0\right), \quad \epsilon'^\mu(l', 0) = \left(\frac{-l}{m_V}, 0, 0, \frac{l^0}{m_V}\right). \quad (\text{A.4})$$

The contributions to the helicity amplitudes are of three kinds (see Sec. II).

• **u- and t-channel exchange.**

For  $W^-W^+$  we only have u-channel bottom exchange leading to

$$A_u^{WW} \rightarrow -\frac{e^2 g_{Wtb}^{2L} (E_t + m_t)}{2(u - m_b^2)} \{T_u^{1L} + T_u^{2L} + T_u^{3L}\}, \quad (\text{A.5})$$

while for  $ZZ$  we have both u-channel and t-channel top exchange leading to

$$\begin{aligned} A_u^{ZZ} &\rightarrow -\frac{e^2 (E_t + m_t)}{2(u - m_t^2)} \{g_{Zt}^{2L} (T_u^{1L} + T_u^{2L} + T_u^{3L}) \\ &\quad + g_{Zt}^{2R} (T_u^{1R} + T_u^{2R} + T_u^{3R}) + g_{Zt}^L g_{Zt}^R T_u^0\}, \\ A_t^{ZZ} &\rightarrow -\frac{e^2 (E_t + m_t)}{2(t - m_t^2)} \{g_{Zt}^{2L} (T_t^{1L} + T_t^{2L} + T_t^{3L}) \\ &\quad + g_{Zt}^{2R} (T_t^{1R} + T_t^{2R} + T_t^{3R}) + g_{Zt}^L g_{Zt}^R T_t^0\}. \end{aligned} \quad (\text{A.6})$$

For both  $W^-W^+$  and  $ZZ$  cases these are expressed in terms of

$$\begin{aligned} T_u^{1L} &= -2(\epsilon'^0 p_t^0 - \epsilon'^1 p_t \sin \theta - \epsilon'^3 p_t \cos \theta)(1 - 2\tau r_t)(r_t + 2\tau') \left( \epsilon^0 \delta_{\tau\tau'} + \sum_{k=1}^3 \epsilon^k S^k \right), \\ T_u^{1R} &= -2(\epsilon'^0 p_t^0 - \epsilon'^1 p_t \sin \theta - \epsilon'^3 p_t \cos \theta)(1 + 2\tau r_t)(r_t - 2\tau') \left( \epsilon^0 \delta_{\tau\tau'} - \sum_{k=1}^3 \epsilon^k S^k \right), \\ T_u^{2L} &= m_t (Y_{11} - Y_{12})(1 + 2\tau r_t)(r_t + 2\tau'), \\ T_u^{2R} &= m_t (Y_{11} - Y_{12})(1 - 2\tau r_t)(r_t - 2\tau'), \\ T_u^0 &= -m_t [Y_{11} r_t (1 + 4\tau\tau') - Y_{12} (2\tau' + 2\tau r_t^2)], \\ T_u^{3L} &= (1 - 2\tau r_t)(r_t + 2\tau')(X_{11} - X_{12}), \\ T_u^{3R} &= (1 + 2\tau r_t)(r_t - 2\tau')(X_{11} + X_{12}), \end{aligned}$$

with

$$\begin{aligned} Y_{11} &= \left( \epsilon'^0 \epsilon^0 - \sum_{k=1}^3 \epsilon'^k \epsilon^k \right) \delta_{\tau\tau'} - i \left[ S^1 (\epsilon'^2 \epsilon^3 - \epsilon'^3 \epsilon^2) + S^2 (\epsilon'^3 \epsilon^1 - \epsilon'^1 \epsilon^3) \right. \\ &\quad \left. + S^3 (\epsilon'^1 \epsilon^2 - \epsilon'^2 \epsilon^1) \right], \\ Y_{12} &= S^1 (\epsilon'^1 \epsilon^0 - \epsilon'^0 \epsilon^1) + S^2 (\epsilon'^2 \epsilon^0 - \epsilon'^0 \epsilon^2) + S^3 (\epsilon'^3 \epsilon^0 - \epsilon'^0 \epsilon^3), \end{aligned}$$

$$\begin{aligned}
X_{11} \mp X_{12} &= l^0(\epsilon'^0 \epsilon^0 + \sum_{k=1}^3 \epsilon'^k \epsilon^k) + l(\epsilon'^0 \epsilon^3 + \epsilon'^3 \epsilon^0) + il(\epsilon'^2 \epsilon^1 - \epsilon'^1 \epsilon^2) \\
&+ S^1 [il(\epsilon'^2 \epsilon^0 - \epsilon'^0 \epsilon^2) + il^0(\epsilon'^2 \epsilon^3 - \epsilon'^3 \epsilon^2) \pm l^0(\epsilon'^0 \epsilon^1 + \epsilon'^1 \epsilon^0) \pm l(\epsilon'^1 \epsilon^3 + \epsilon'^3 \epsilon^1)] \\
&+ S^2 [il(\epsilon'^0 \epsilon^1 - \epsilon'^1 \epsilon^0) + il^0(\epsilon'^3 \epsilon^1 - \epsilon'^1 \epsilon^3) \pm l^0(\epsilon'^0 \epsilon^2 + \epsilon'^2 \epsilon^0) \pm l(\epsilon'^2 \epsilon^3 + \epsilon'^3 \epsilon^2)] \\
&+ S^3 [il^0(\epsilon'^1 \epsilon^2 - \epsilon'^2 \epsilon^1) + l^0(\epsilon'^0 \epsilon^3 + \epsilon'^3 \epsilon^0) \pm l(\epsilon'^0 \epsilon^0 - \sum_{k=1}^3 \epsilon'^k \epsilon^k) \pm l(\epsilon'^3 \epsilon^3 + \epsilon'^3 \epsilon'^3)] ,
\end{aligned}$$

and

$$\begin{aligned}
S^1 &= \cos \theta (\delta_{\tau_+} \delta_{\tau'_-} + \delta_{\tau_-} \delta_{\tau'_+}) + \sin \theta (\delta_{\tau_+} \delta_{\tau'_+} - \delta_{\tau_-} \delta_{\tau'_-}) , \\
S^2 &= -i(\delta_{\tau_+} \delta_{\tau'_-} - \delta_{\tau_-} \delta_{\tau'_+}) , \\
S^3 &= -\sin \theta (\delta_{\tau_+} \delta_{\tau'_-} + \delta_{\tau_-} \delta_{\tau'_+}) + \cos \theta (\delta_{\tau_+} \delta_{\tau'_+} - \delta_{\tau_-} \delta_{\tau'_-}) .
\end{aligned}$$

For the t-channel contribution the  $T_t^i$  terms are obtained from the  $T_u^i$  ones, by the interchanges

$$u \rightarrow t , \quad \epsilon \rightarrow \epsilon' , \quad l \rightarrow -l .$$

- **s-channel  $V = \gamma, Z$  exchange, only for  $WW$ .**

$$\begin{aligned}
A_{s,V}^{WW} &\rightarrow \frac{e^2 g_V (E_t + m_t)}{2(s - m_V^2 + im_V \Gamma_V)} \left\{ -\frac{4ll^0}{m_W} \delta_{\lambda'0} \left[ \epsilon^0 \delta_{\tau\tau'} + \sum_{k=1}^3 \epsilon^k S^k \right] + \frac{4ll^0}{m_W} \delta_{\lambda 0} \left[ \epsilon'^0 \delta_{\tau\tau'} \right. \right. \\
&\left. \left. + \sum_{k=1}^3 \epsilon'^k S^k \right] - 2l\epsilon.\epsilon' S^3 \right\} \cdot \left\{ g_{Vt}^L (1 - 2\tau r_t)(r_t + 2\tau') + g_{Vt}^R (1 + 2\tau r_t)(r_t - 2\tau') \right\} .
\end{aligned}$$

- **s-channel  $H$  exchange, for both  $W^-W^+$  or  $ZZ$**

$$A_{s,H}^{XX} \rightarrow \frac{2e^2 g_{HXX} g_{Htt} p_t}{s - m_H^2 + im_H \Gamma_H} (\epsilon.\epsilon') \delta_{\tau\tau'} ,$$

with  $g_{HXX} = g_{HWW}, g_{HZZ}$ .

## References

- [1] M.E. Peskin, Ann.Phys.(N.Y.)**528**,20(2016). M. Muhlleitner, arXiv:1410.5093. Ben Gripaios, arXiv:1503.02636, arXiv:1506.05039.
- [2] H. Terazawa, Y. Chikashige and K. Akama, Phys. Rev. **D15**, 480 (1977); for other references see H. Terazawa and M. Yasue, Nonlin.Phenom.Complex Syst. **19**,1(2016); J. Mod. Phys. **5**, 205 (2014).
- [3] G. Panico and A. Wulzer, Lect.Notes Phys. **913**,1(2016).
- [4] B.Patt and F. Wilczek, arXiv: hep-ph/0605188.
- [5] R. Contino, T. Kramer, M. Son and R. Sundrum, J. High Energy Phys. 05(**2007**)074.
- [6] M.S. Chanowitz and M.K. Gaillard, Phys. Lett. **B142**, 85 (1984); G.L. Kane, W.W. Repko and W.B. Rolnick, Phys. Lett. **B148**, 367 (1984); S. Dawson, Nucl. Phys. **B249**, 42 (1985).
- [7] R.P. Kauffman, Phys. Rev. **D41**, 3343 (1990).
- [8] M. Gintner and S. Godfrey, arXiv: 9612342 [hep-ph], eConf.0960625(1996)STC 130, proceedings of the 1996 Summer Study on New Directions for High-Energy Physics, Snowmass 1996. C.-P. Yuan, Nucl. Phys. **B310**, 1 (1988).
- [9] E. Accomando et al. Phys. Rept. **299**, 1 (1998).
- [10] M. Capdequi-Peyranere et al, Z. f. Phys. **C41**, 1988 (99).
- [11] M. Jacob and G.C. Wick, Annals of Phys. **7**, 404 (1959), Annals of Phys. **281**, 774 (2000).
- [12] G.J. Gounaris and F.M. Renard, Phys. Rev. Lett. **94**, 131601 (2005); Phys. Rev. **D73**, 097301 (2006).
- [13] J.A. Aguilar Saavedra, Nucl. Phys. **B821**, 215 (2009).
- [14] G. Passarino and M. Veltman, Nucl. Phys. **B160**, 151 (1979).
- [15] G.J. Gounaris and F.M. Renard, Acta Phys. Polon. **42**, 2107 (2011); Phys. Rev. **D86**, 013003 (2012); Phys. Rev. **D90**, 073007 (2014).
- [16] G. Aad et al.[ATLAS Collaboration], Reports No. ATLAS-CONF-2015-081(2015) and No. ATLAS-CONF-2016-018.
- [17] S. Chatrchyan et al.[CMS Collaboration], Reports No. CMS-PAS-EXO-15-004(2015) and No. CMS-PAS-EXO-16-018.

- [18] See for example [http : //indico.cern.ch/event/432527/contributions/1072336/attachments/1321033/1981068/BLATLAS\\_HighMassDiphotons\\_CHEP2016.pdf](http://indico.cern.ch/event/432527/contributions/1072336/attachments/1321033/1981068/BLATLAS_HighMassDiphotons_CHEP2016.pdf)  
and [http : //indico.cern.ch/event/432527/contributions/1072431/attachments/1320985/1980991/chiara\\_chep.pdf](http://indico.cern.ch/event/432527/contributions/1072431/attachments/1320985/1980991/chiara_chep.pdf)
- [19] F. Larios, T. Tait and C.-P. Yuan, Phys. Rev. **D57**, 3106 (1998).
- [20] D. d'Enterria, arXiv: 1602.05043[hep-ex] and its Refs.1-4.



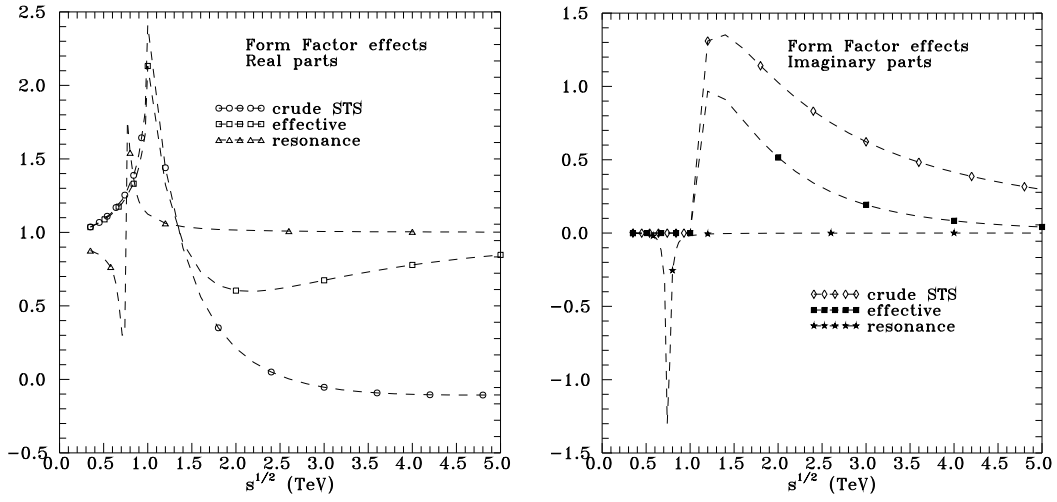


Figure 1: The shapes of the real parts (left panel) and imaginary parts (right panel) of the  $Ht\bar{t}$  form factors; the *crude* lines are based on (16) and (17), the *effective* lines on (19) and (17) and the *resonance* lines are based on (20).

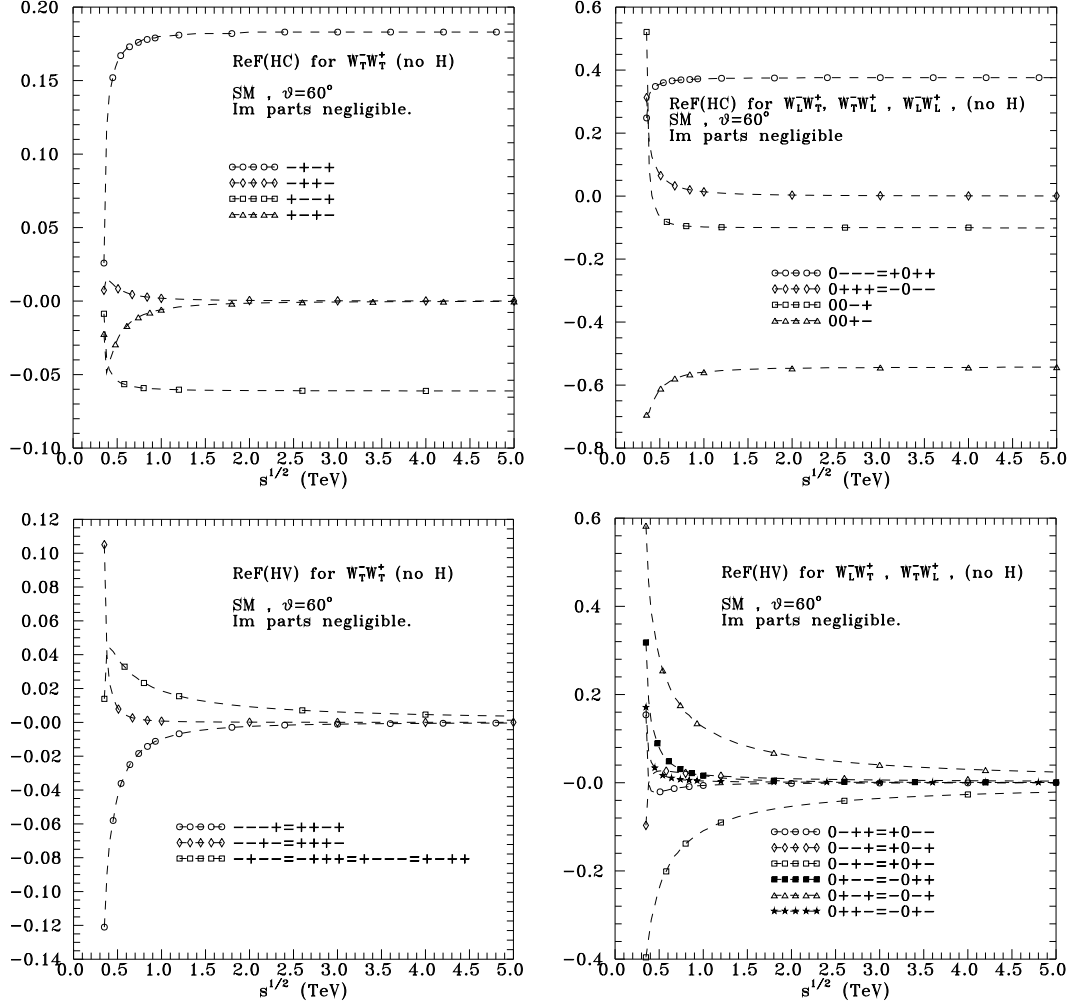


Figure 2: Energy dependence of the H-insensitive tree-level SM amplitudes for  $W_{\lambda}^{-} W_{\lambda'}^{+} \rightarrow t_{\tau} \bar{t}_{\tau'}$ . Upper panels are for the HC amplitudes of (23), and lower panels are for the HV ones of (24) at  $\theta = 60^{\circ}$ . Left panels present TT amplitudes, while right panels involve amplitudes containing at least one longitudinal  $W$ .

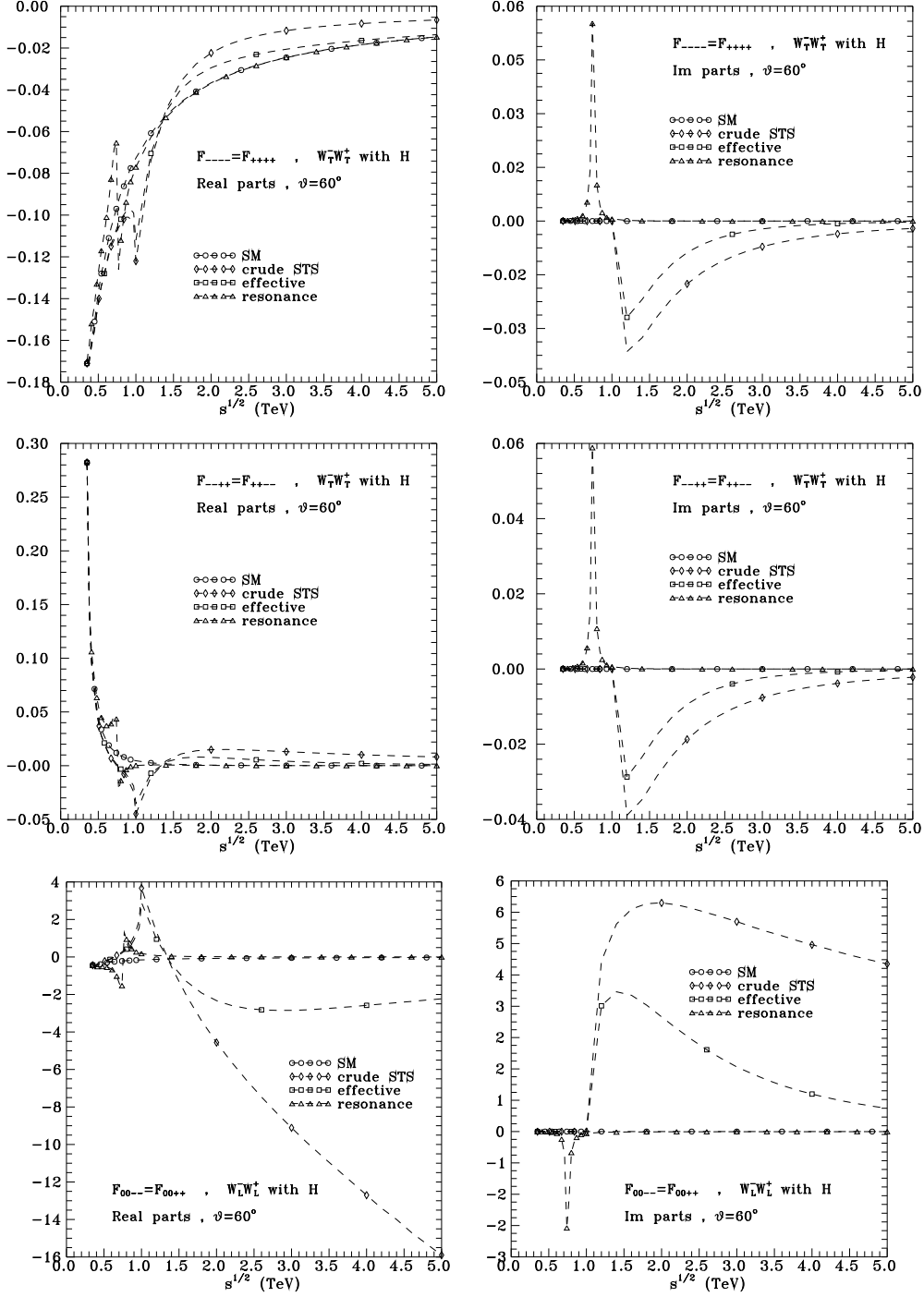


Figure 3: The SM results and the effects of the anomalous  $Htt$  form factor on the form factor sensitive amplitudes  $W_{\lambda}^{-}W_{\lambda'}^{+} \rightarrow t_{\tau}\bar{t}_{\tau'}$  listed in (25). real (imaginary) parts are shown in the left (right) panels respectively. The definition of *crude STS*, *effective* and *resonance* form factor models, as in Fig.1.

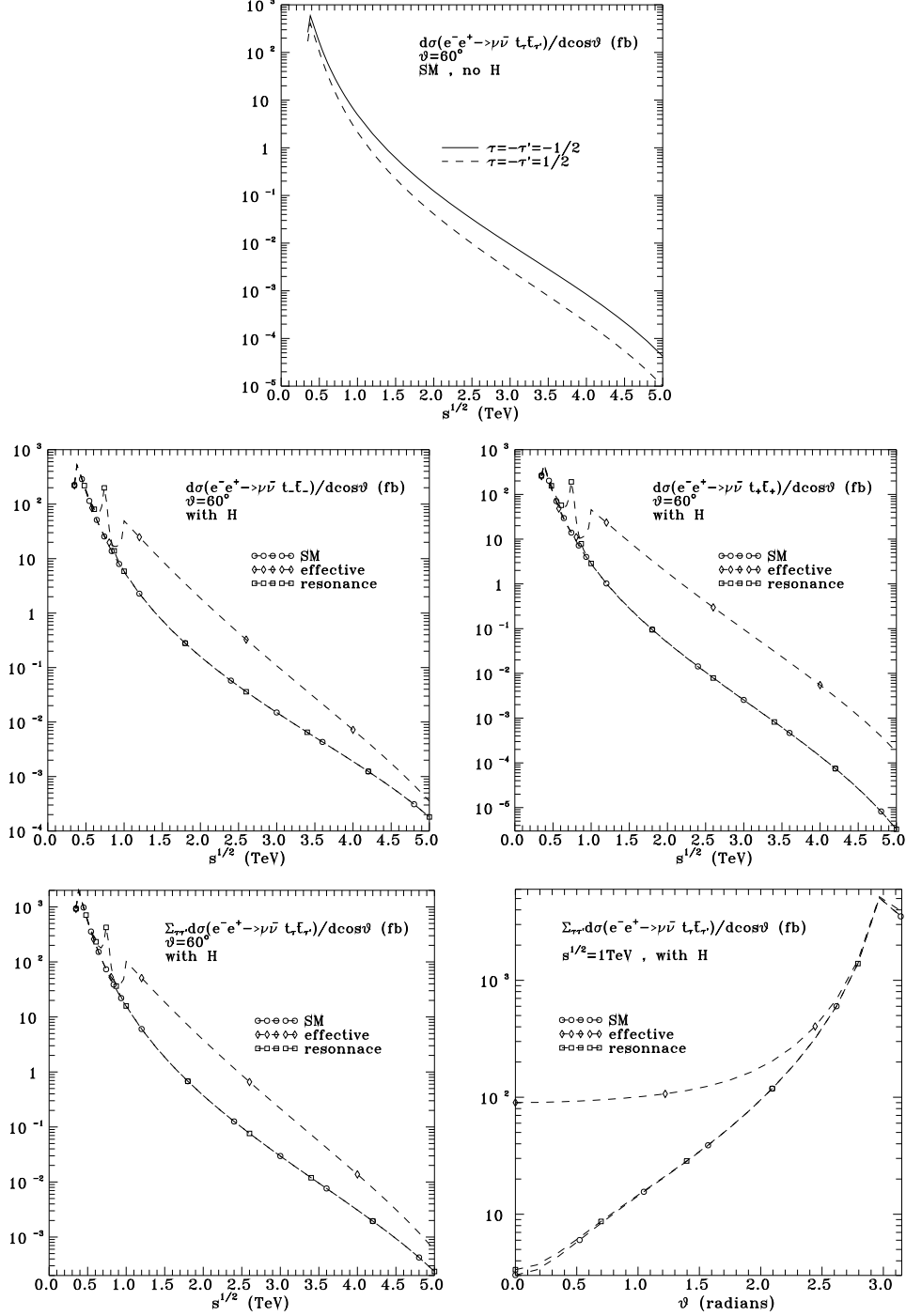


Figure 4:  $d\sigma(e^-e^+ \rightarrow \nu\bar{\nu}' t_\tau \bar{t}_{\tau'})/d\cos\theta$  cross sections. The upper panel gives energy dependencies for (left-right) and (right-left)  $t\bar{t}$  helicities, while middle panels for (left-left) and (right-right)  $t\bar{t}$  helicities, always at  $\theta = 60^\circ$ . The lower panels give energy (at  $\theta = 60^\circ$ ) and angular (at  $\sqrt{s} = 1\text{ TeV}$ ) dependencies when  $t\bar{t}$ -helicities are not observed. The contribution from the  $H$  form factors of the three cases of Fig.1, exist only for the  $t\bar{t}$  polarizations contributing to the middle and lower panels.

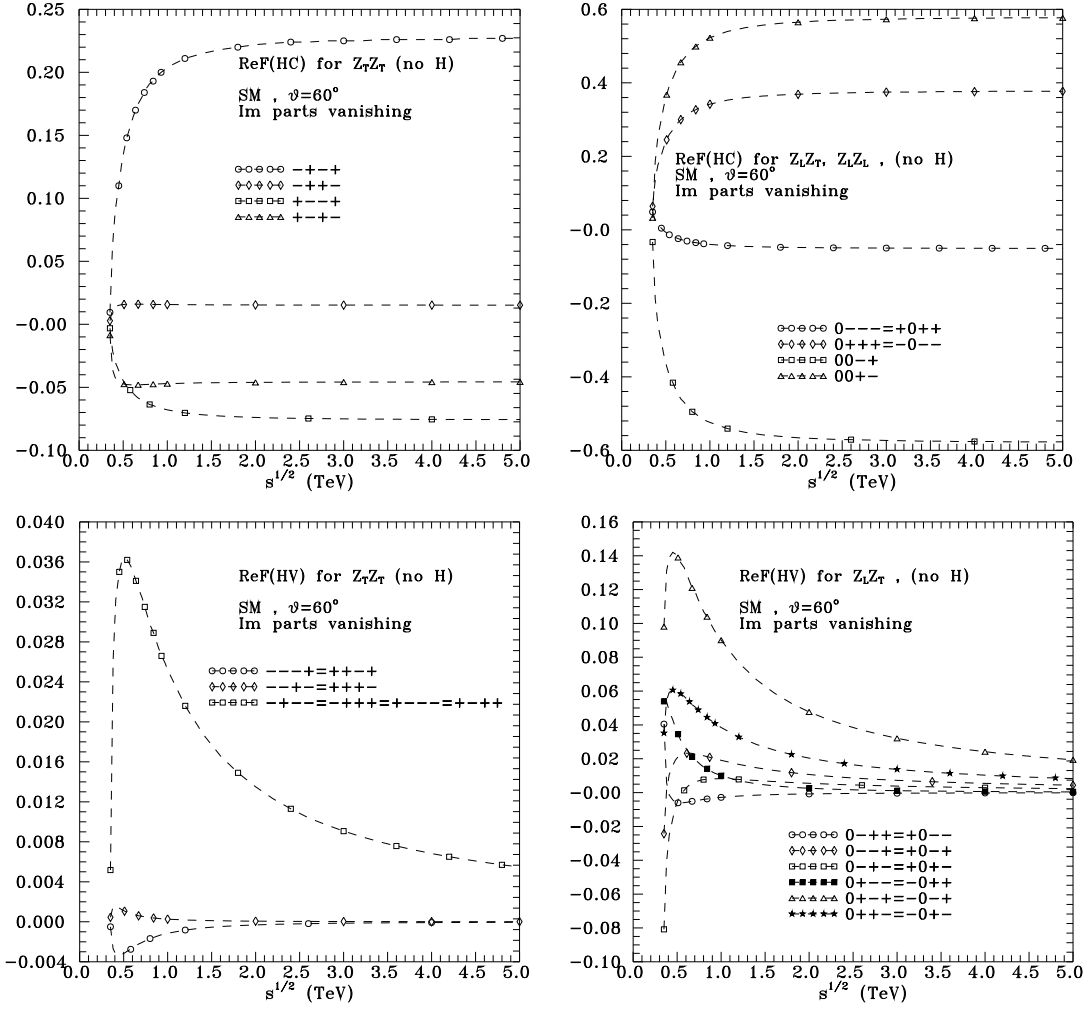


Figure 5: Energy dependence of the H-insensitive tree-level SM amplitudes for  $Z_\lambda Z_{\lambda'} \rightarrow t_\tau \bar{t}_{\tau'}$  at  $\theta = 60^\circ$ . Upper panels are for the HC amplitudes in (26) and lower panels are for the HV ones in (27).

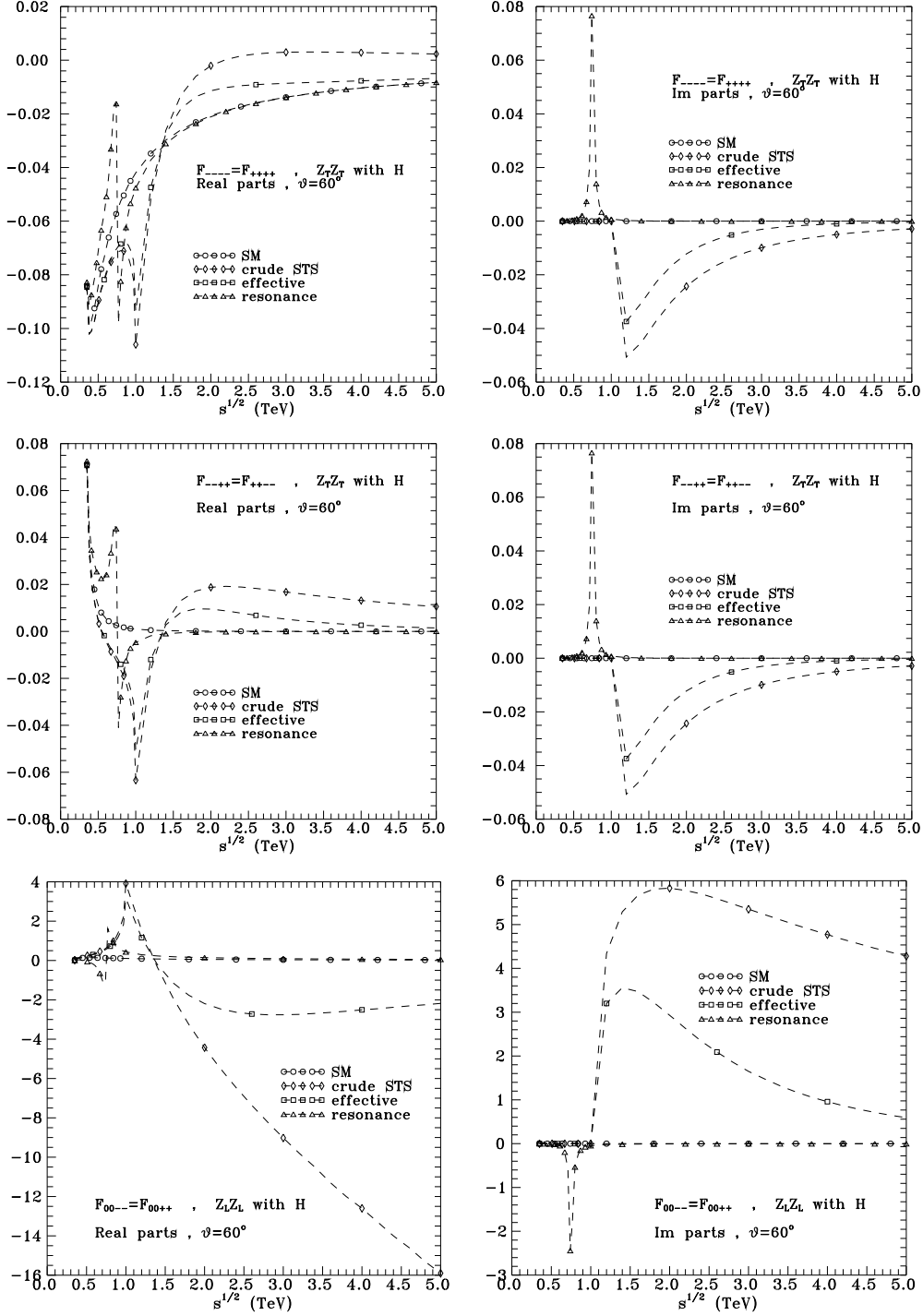


Figure 6: The SM results and the effects of the anomalous  $Htt$  form factor on the sensitive to it amplitudes  $Z_\lambda Z_{\lambda'} \rightarrow t_\tau \bar{t}_\tau$ , listed in (28). Real (imaginary) parts are shown in the left (right) panels respectively. The definition of *crude STS*, *effective* and *resonance* form factor models, as in Fig.1.

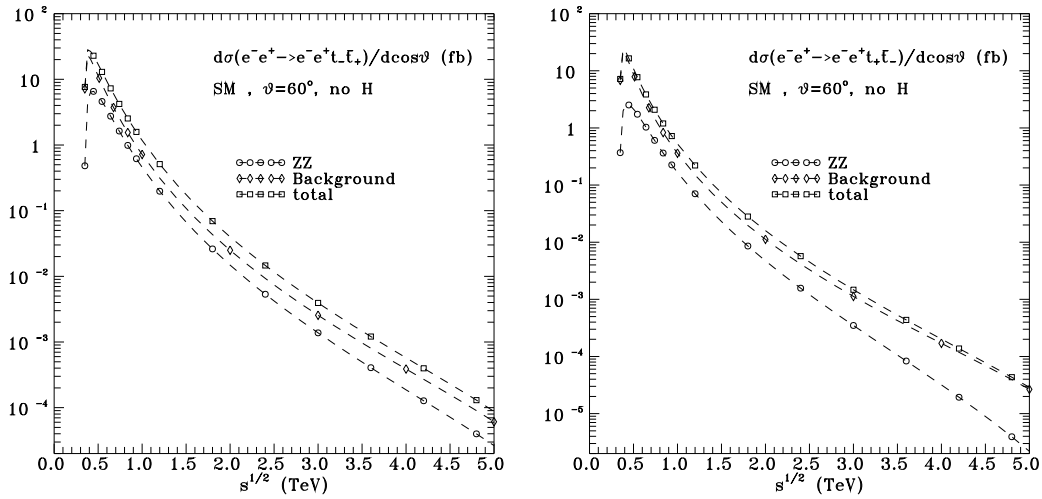


Figure 7: Energy dependencies of the differential cross sections for  $d\sigma(e^-e^+ \rightarrow e^-e^+t_\tau\bar{t}_{\tau'})/d\cos\theta$  at  $\theta = 60^\circ$ . The  $ZZ$  intermediate state, the *background* induced by anything non- $ZZ$ , and the complete result denoted as "total" are separately given. The left (right) panel corresponds to  $\tau = -\tau' = -1/2$  ( $\tau = -\tau' = +1/2$ ) and they both contain no  $H$  contribution.

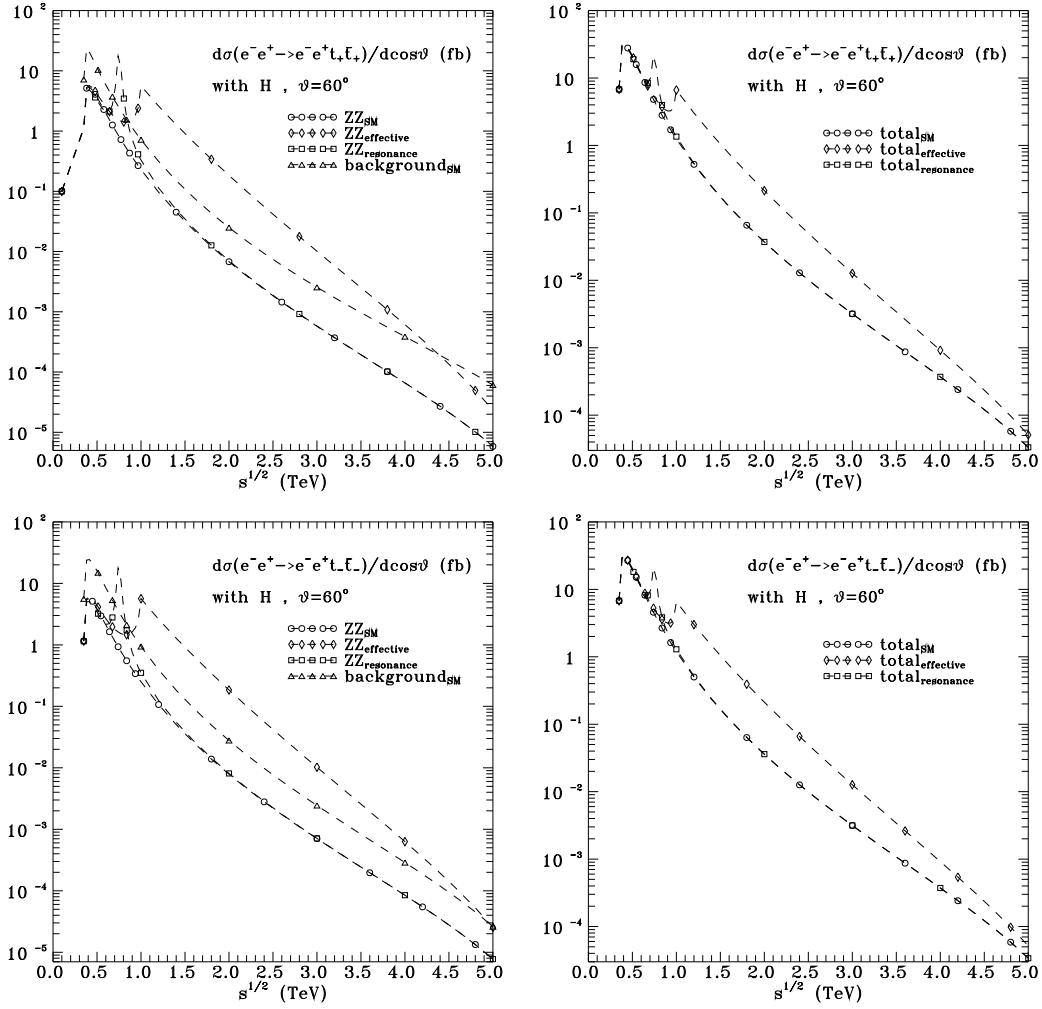


Figure 8: Differential cross sections as in Fig.7, with upper and lower panels respectively corresponding to  $\tau = \tau' = \pm 1/2$  and both receiving  $H$  form factor contributions (see Fig.1) modifying the  $ZZ$  (left) and the "total" (right) panel results.



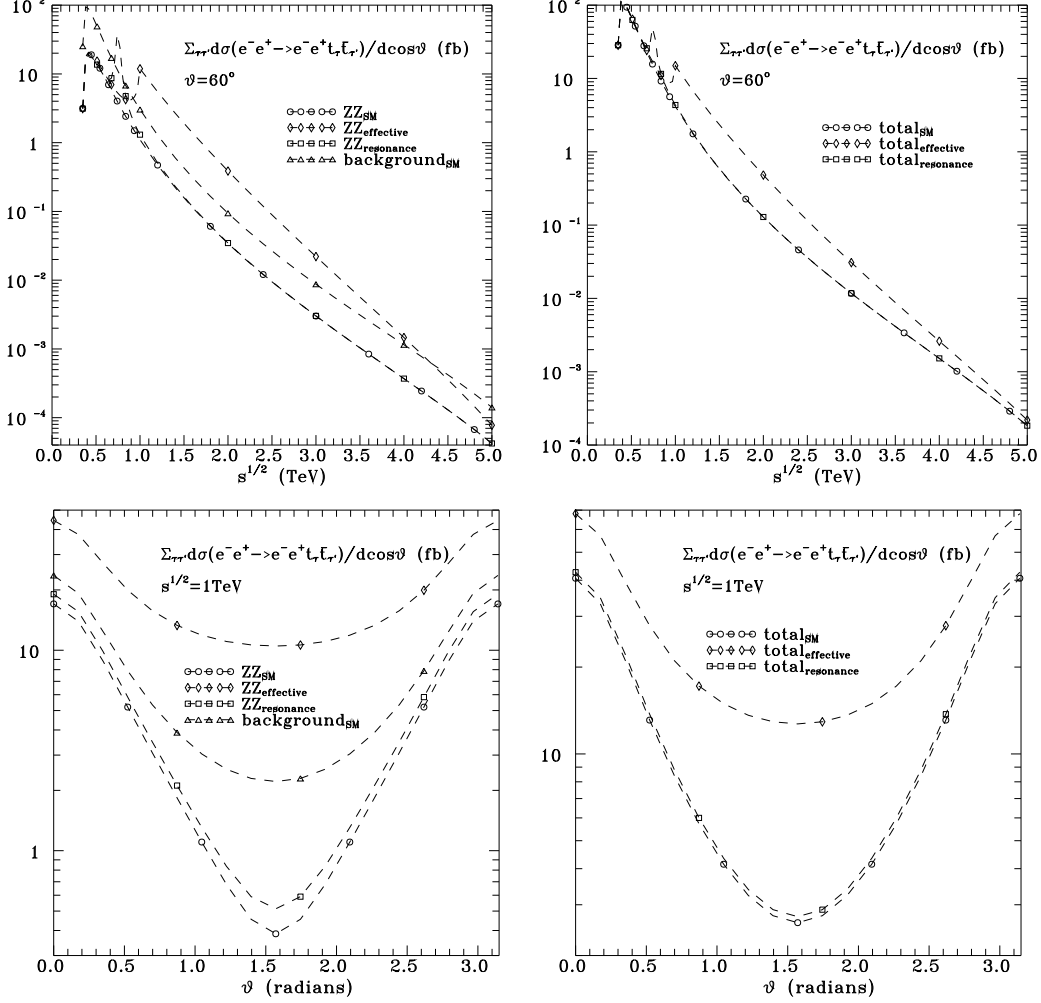


Figure 9: Energy dependencies at  $\theta = 60^\circ$  (upper panels) and angular dependencies at  $\sqrt{s} = 1\text{TeV}$  (lower panels) of the unpolarized differential cross sections for  $\sum_{\tau\tau'} d\sigma(e^-e^+ \rightarrow e^-e^+t_\tau\bar{t}_{\tau'})/d\cos\theta$ . The  $ZZ$  intermediate state, the *background* induced by anything non- $ZZ$ , and the complete result indicated as "total" are separately given in SM and after including the  $H$  form factor (see Fig.1) contribution.